Protocol for intraoperative assessment of the human cerebrovascular glycocalyx

NEOPLASIA
www.neoplasia.com

Volume 19 Number 11 November 2017 pp. 896–907 896

Nilotinib Enhances Tumor Angiogenesis and Counteracts VEGFR2 Blockade in an Orthotopic Breast Cancer Xenograft Model with Desmoplastic Response

Sara Zafarnia[*], Jessica Bzyl-Ibach[*], Igor Spivak[*], Yongping Li[*], Susanne Koletnik[*], Dennis Doleschel[*], Anne Rix[*], Sibylle Pochon[†], Isabelle Tardy[†], Seena Koyadan[‡], Marc van Zandvoort[§,¶], Moritz Palmowski[#], Fabian Kiessling[*] and Wiltrud Lederle[*]

[*]Institute for Experimental Molecular Imaging, Medical Faculty, RWTH Aachen University, Aachen, Germany; [†]Bracco Suisse SA, Geneva, Switzerland; [‡]Core Facility Two-Photon Imaging, Interdisciplinary Center for Clinical Research Aachen, Germany; [§]Institute for Molecular Cardiovascular Research (IMCAR), RWTH Aachen University Clinic, Aachen, Germany; [¶]Department of Genetics and Cell Biology, Cardiovascular Research Institute Maastricht (CARIM), Maastricht University, Maastricht, the Netherlands; [#]Academic Radiology Baden-Baden, Diagnostic and Interventional Radiology, University Medical Center Heidelberg, Germany

Abstract

Vascular endothelial growth factor (VEGF)/VEGF receptor (VEGFR)-targeted therapies predominantly affect nascent, immature tumor vessels. Since platelet-derived growth factor receptor (PDGFR) blockade inhibits vessel maturation and thus increases the amount of immature tumor vessels, we evaluated whether the combined PDGFR inhibition by nilotinib and VEGFR2 blockade by DC101 has synergistic therapy effects in a desmoplastic breast cancer xenograft model. In this context, besides immunohistological evaluation, molecular ultrasound imaging with BR55, the clinically used VEGFR2-targeted microbubbles, was applied to monitor VEGFR2-positive vessels noninvasively and to assess the therapy effects on tumor angiogenesis. DC101 treatment alone inhibited tumor angiogenesis, resulting in lower tumor growth and in significantly lower vessel density than in the control group after 14 days of therapy. In contrast, nilotinib inhibited vessel maturation but enhanced VEGFR2 expression, leading to markedly increased tumor volumes and a significantly higher vessel density. The combination of both drugs led to an almost similar tumor growth as in the DC101 treatment group, but VEGFR2 expression and microvessel density were higher and comparable to the controls. Further analyses revealed significantly higher levels of tumor cell–derived VEGF in nilotinib-treated tumors. In line with this, nilotinib, especially in low doses, induced an upregulation of VEGF and IL-6 mRNA in the tumor cells *in vitro*, thus providing an explanation for the enhanced angiogenesis observed in nilotinib-treated tumors *in vivo*. These findings suggest that nilotinib inhibits vessel maturation but counteracts the effects of antiangiogenic co-therapy by enhancing VEGF expression by the tumor cells and stimulating tumor angiogenesis.

Neoplasia (2017) 19, 896–907

Introduction

The vascular endothelial growth factor (VEGF) has been identified as a key driver of tumor angiogenesis [1], and various drugs have been developed that block VEGF/VEGF receptor (VEGFR) signaling. However, different modes of resistance to anti-VEGF/VEGFR therapies have been observed in preclinical cancer models and in cancer patients, e.g., intrinsic resistance in which tumors show no therapy response from the beginning on or evasive resistance, whereby

Abbreviations: VEGF, vascular endothelial growth factor; VEGFR, vascular endothelial growth factor receptor; α-SMA, α-smooth muscle actin; PDGF, platelet-derived growth factor; PDGFR, platelet-derived growth factor receptor; TPLSM, two-photon laser scanning microscopy; IL-6, interleukin-6

Address all Correspondence to: Dr. Wiltrud Lederle, PhD, Institute for Experimental Molecular Imaging, RWTH-Aachen University, Pauwelsstrasse 30, 52074 Aachen, Germany.
E-mail: wlederle@ukaachen.de

Received 17 January 2017; Revised 25 August 2017; Accepted 28 August 2017

1476-5586
http://dx.doi.org/10.1016/j.neo.2017.08.009

inhibition of VEGF signaling only leads to a transient therapeutic benefit, often followed by tumor progression [2–4].

One mode of resistance to VEGF/VEGFR inhibition can be attributed to blood vessel maturation [2,3]. Mature vessels show a low vulnerability towards anti-VEGF/VEGFR therapy due to the close association of α-smooth muscle actin (α-SMA)–expressing pericytes or smooth muscle cells with the endothelium. These perivascular cells stabilize the endothelial tubes, mediate endothelial survival, and render them independent of VEGF secreted by tumor or stromal cells [5–7]. The recruitment of pericytes or smooth muscle cells to the vessels and thus vessel maturation are dependent on platelet-derived growth factor (PDGF)-B/PDGF receptor (PDGFR)-β signaling [8]. In consequence, targeting VEGFR2 and PDGFR-β signaling may inhibit both angiogenesis and vessel maturation and thus more efficiently affect newly formed tumor vessels and more strongly impair tumor growth. An improved therapeutic efficacy was observed in a transgenic model of pancreatic islet cancer by combined inhibition of VEGFR- and PDGFR-β signaling [7]. Whereas sole VEGFR inhibition was ineffective in larger, well-vascularized pancreatic islet tumors at advanced stages, combined treatment with a PDGFR-β inhibitor resulted in profound tumor vessel regression and a strong reduction in tumor mass [7].

For the assessment of therapy effects in the clinics, noninvasive imaging is inevitable, providing reliable information on morphological, functional, and molecular alterations during the treatment course. For imaging of tumor angiogenesis, which is a crucial prerequisite for the growth and progression of solid tumors and an important target for tumor therapy, different modalities are used in the clinics such as dynamic contrast-enhanced magnetic resonance imaging/computed tomography, positron emission tomography, single photon emission computed tomography, or contrast-enhanced ultrasound imaging [9–12]. Contrast-enhanced ultrasound imaging has the advantage that it is easy to handle, allows low-cost analyses, and can provide functional and molecular data on the tumor vasculature [13,14]. For the analyses of tumor vascularization and perfusion, contrast-enhanced ultrasound imaging with nontargeted microbubbles has emerged as a sensitive and well-suited method [15,16]. The application of microbubbles that bind to molecular markers expressed on the endothelium, referred to as molecular ultrasound imaging, allows the noninvasive characterization of tumor angiogenesis at the molecular level [17–20]. Especially, microbubbles targeting VEGFR2 have shown promise in assessing the effects of anticancer therapies including antiangiogenic treatments [18,19,21]. Among them, there is one lipopeptide-based microbubble, BR55, which has shown a high sensitivity in depicting the decrease in angiogenesis in response to antiangiogenic therapy in preclinical models and has been already administered in patients [22–26].

In this study, we performed combination therapy targeting VEGFR2 by DC101 and PDGFR signaling by nilotinib in a breast cancer xenograft with desmoplastic stroma in order to concomitantly inhibit tumor angiogenesis and vessel maturation. The effects of the combination therapy were compared with the single therapies. Nilotinib (Tasigna) is a potent inhibitor of the PDGFRs, with similar IC50 values as imatinib (Gleevec), but has almost no effect on VEGFR2 [27,28]. In order to noninvasively assess the effects of the therapies on tumor angiogenesis, molecular ultrasound imaging with BR55 was applied. Imaging data were compared with immunohistochemistry at the end of therapy.

Material and Methods

Breast Cancer Xenografts

Animal experiments were approved by the governmental review committee on animal care. Human breast adenocarcinoma cells (MCF-7, CLS) were used to induce tumor xenografts. Female CD1 nude mice (Charles River) received subcutaneous estrogen pellets (1.5 mg/pellet; 90-day release; Innovative Research of America) into the left lateral side of the neck followed by an orthotopic injection of 5×10^6 MCF-7 cells into the mammary fat pad [24]. Tumor growth was monitored by caliper measurements every second day, and tumor volumes were determined using the formula $1/6 \times \pi \times \text{width}^2 \times \text{length}$. Tumor volume was normalized to the initial tumor volume on day 0.

Therapy Design

When tumors reached 3 to 4 mm in diameter, the animals were randomly divided into four treatment groups with six animals each ($n = 6$ per group). One group received every second day 800 μg of the murine VEGFR2 neutralizing antibody DC101 (BioXCell) in 110 μl PBS by intraperitoneal injection. The second group was treated every day with 75 mg/kg body weight of the PDGFR inhibitor nilotinib (Tasigna®, Novartis) orally by gavage. The content of the capsule containing nilotinib was dissolved in a 0.5% hydroxypropylmethylcellulose, 0.05% Tween 80 solution. The third treatment group received a combination of DC101 and nilotinib, each administered as described above. Animals of the control group received solvents without pharmaceutically active components every day. Therapy duration was 14 days.

Longitudinal Assessment of the VEGFR2 Expression by Molecular Ultrasound Imaging

Ultrasound imaging of the tumors was performed at day 7 and 14 of treatment using the Vevo 2100 small-animal high-resolution ultrasound system with a 21-MHz transducer (MS-250, VisualSonics) in order to assess the therapy effects on tumor angiogenesis. VEGFR2-targeted microbubbles (BR55, Bracco Suisse SA) were used as molecular ultrasound contrast agent. Endothelial VEGFR2 expression within the tumors was measured using the "destruction-replenishment" method, as described previously [29]. In brief, mice were anesthetized with inhalation of 2% isoflurane in oxygen-enriched air, and 1×10^8 BR55 microbubbles were injected *via* the tail vein, followed by a saline flush. The injection was monitored by imaging in contrast mode the central plane of the tumor for 30 seconds at 18 MHz and 4% transmit power with a frame rate of 10 Hz. Before applying the destructive pulse, microbubbles were allowed to circulate for 8 minutes to give enough time for binding to the VEGFR2. A sequence of images was taken for 10 seconds followed by the application of a high-amplitude pulse that destroyed all microbubbles within the slice. Immediately after the destructive pulse, images were acquired at 10 Hz for another 40 seconds to assess the vascular replenishment of residual circulating microbubbles. The signal intensity (SI) after the destructive pulse was subtracted from the SI before the destructive pulse in order to determine the SI of VEGFR2-bound microbubbles.

At day 14, animals were injected with 15 mg/kg FITC-labeled lectin (Vector Laboratories, Inc.) to label perfused vessels. Ten minutes after injection, mice were sacrificed. Tumors were resected, halved in the middle, and cryoconserved in Tissue-Tek (Sakara) for histologic analysis.

Antibodies

The following primary antibodies were used: rat anti-mouse CD31 (BD Biosciences), goat anti-mouse VEGFR2 (R&D Systems), rabbit anti-human PDGFR-β (Santa Cruz Biotechnology), goat anti-mouse VEGF (R&D Systems), goat anti-human VEGF (R&D Systems), and biotinylated anti-α-smooth muscle actin (α-SMA, Progen). Secondary antibodies were obtained from Dianova and Hoechst 33258 bisbenzimide for staining of cell nuclei from Sigma-Aldrich.

Indirect Immunofluorescence

Frozen sections of the central part of the tumor, located within the ultrasound plane, were used for immunofluorescent staining. Tumor sections were fixed for 5 minutes in 80% methanol and 2 minutes in acetone at −20°C. The staining was performed as described previously [30].

Fluorescent microphotographs were acquired with an epifluorescence microscope (Axio Imager.M2, Zeiss) and a high-resolution camera (AxioCamMRm Rev.3, Zeiss). Quantitative analysis was performed in five to seven microphotographs per section (including top, bottom, sides, and center of each section) using the AxioVisionRel 4.8 software (Zeiss). The VEGFR2 expression was quantified by determining the VEGFR2-positive area fraction. In order to determine functional tumor blood vessels, lectin-positive area fractions were quantified. In addition, the microvessel density was assessed by quantifying the CD31-positive area fractions. To determine vessel maturation, the amount of α-SMA–positive cells and CD31-positive vessels was counted manually, and the percentage of α-SMA–positive cells per CD31-positive vessels was calculated. The amount of myofibroblasts was assessed by quantitative determination of the PDGFR-β– and of α-SMA–positive area fraction (excluding the vessels). VEGF expression was quantified by calculating the ratio of the VEGF-positive to the DAPI-positive area fraction.

Two-Photon Laser Scanning Microscopy (TPLSM)

To analyze the three-dimensional structure of the tumor vasculature, TPLSM was performed. The second halves of the tumor tissues were cut into 200-μm–thick slices. FITC-labeled vessels were imaged using an Olympus Fluoview FV1000-MPE multiphoton system coupled with MaiTaiDeepSee (140 fs) Ti:Sapphire laser at an excitation wavelength of 800 nm and 25× water dipping objective (numerical aperture = 1.05, working distance = 2 mm). For the detection of emitted fluorescent signals, two ultrasensitive external nondescanned PMT detectors were tuned to the corresponding parts of the emission spectra of FITC (490-540 nm). Images of 1024 × 1024 pixels were obtained at successive 1.5-μm depth positions in *xy* directions using the image acquisition software FV10-ASW Ver 3.0 (Olympus).

Effects of Nilotinib and VEGFR2 Blockade on Endothelial Tube Formation In Vitro

The direct effects of nilotinib on endothelial tube formation were analyzed *in vitro* using HUVEC (Promocell) and the "*In Vitro* Angiogenesis Assay Kit" (Abcam). In brief, cells (1.5×10^4 per well) were seeded in 96-well plates (VWR) precoated with Extracellular Matrix Gel (Abcam) for 1 h (37°C) and grown in medium (VascuLife VEGF, Lifeline Cell Technologies) supplemented with 2 μM and 20 μM of nilotinib [dissolved in 2% (v/v) of DMSO, Sigma-Aldrich]. DMSO (2%) and medium alone were used as controls ($n = 3$ per culture and treatment condition). Tube formation was analyzed after 5 hours using an inverse phase contrast light microscope (Axiovert 40C, Zeiss) and by counting the number of tubes (Image J Software).

Effects of Nilotinib on mRNA Expression of HUVEC and MCF-7 In Vitro

HUVECs (Promocell) were cultured in VascuLife VEGF medium (LifeLine Cell Technology), MCF-7 cells were grown in DMEM with β-estradiol (1 nM, Sigma-Aldrich). For analysis of mRNA expression, the cells were seeded in numbers of 1×10^6 per flask (T75, Greiner Bio-One GmbH). After 24 hours, the cells were washed with PBS and treated for 6 hours with different doses of nilotinib. For HUVEC, 2 μM of nilotinib was used [dissolved in 0.0025% (v/v) DMSO, respectively]. MCF-7 cells received nilotinib in concentrations of 2 μM, 0.5 μM, and 0.25 μM, respectively [dissolved in 0.0025% (v/v)]. Cells treated with DMSO (0.0025%) were used as controls ($n = 3$ per culture and treatment condition). Thereafter, the cells were removed from the flask by scraping, collected in cell culture tubes, and centrifuged at 1000 rpm for 5 minutes. Afterwards, cells were washed with PBS and centrifuged for 5 minutes at 1000 rpm. Cell pellets were frozen at −80°C. Cells were lysed and total RNA was isolated using the EURx GeneMatrix Purification Kit (Roboklon) according to the manufacturer's instructions. The RNA concentration was determined using the NanoDrop 2000 spectrophotometer (Thermo Scientific).

cDNA was generated using the iScript cDNA Synthesis Kit (Bio-Rad). For quantitative polymerase chain reaction (qPCR), cDNA (0.1 μg) was amplified using the SsoAdvanced Universal SYBR Green Supermix (Bio-Rad) and the Thermocycler CFX 96 touch (Bio-Rad). Crossing point values were calculated automatically using the CFX Manager 3.1 software (Bio-Rad). PCR efficiency was assumed to be 100%. Expression of β-actin was analyzed as housekeeping gene. Gene expression normalized to the housekeeping gene (β-actin) was calculated using the $2^{-\Delta\Delta CT}$ method.

The following primers were used (all from Eurofins): hVEGF_for 5′-CGAGGGCCT-GGAGTGTGT-3′, hVEGF_rev 5′-GGCCTT GGTGAGGTTTGATC-3′, hIL-6 for 5′-GG-CATCTCAGCCCT GAGAAAG-3′, hIL-6 rev 5′-CACCAGGCAAGTCTCCTCATT-3′, hVEGFR2_for 5′-GACGGACAGTGGTATGGTT-3′, hVEGF R2_rev 5′-CCGAGTCAGGCT-GGAGAA-3′, hRAF1_for 5′-CCA GTCCCTCATCTGAAGGTTCC-3′, hRAF1_rev 5′-GTG-GACA GCATCACTTCACTGGC-3′, hβ-actin_for 5′-TCACCCACACT GTGCCCATCT-ACGA-3′, hβ-actin_rev 5′-CAGCGGAACCGC TCATTGCCAATGG-3′.

Statistical Analysis

Data are presented as mean values ± standard deviation. For comparison of the different treatment groups in the *in vivo* experiments, one-way analysis of variance was performed followed by a Bonferroni correction for multiple testing (*$P < .05$, **$P < .01$, ***$P < .001$). Statistical analyses were performed using GraphPad Prism 5.0 (GraphPad Software).

Results

Nilotinib Treatment Enhances Tumor Growth

In the control group, tumors showed a continuous growth, leading to a four-fold increase in volume after 14 days. Tumor growth in the DC101 and combined treatment group was lower as compared to the control group. In the nilotinib group, the mean tumor volume strongly increased from day 10 to day 14. However, the differences between the groups were not significant (Figure 1).

Nilotinib Treatment Enhances Tumor Angiogenesis

Assessment of tumor angiogenesis at treatment day 7 and 14 by molecular ultrasound imaging with BR55 revealed the highest

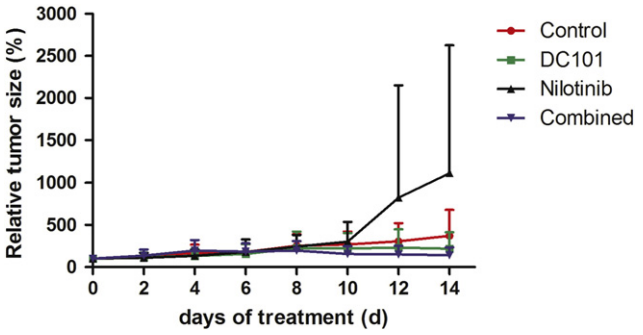

Figure 1. Nilotinib treatment enhances tumor growth. Mean of normalized tumor volumes (± standard deviation) over time: The mean tumor volume in the control group showed an almost four-fold increase during the whole observation period, whereas tumor growth was inhibited in the DC101 and combination therapy group. Nilotinib-treated tumors markedly increased in volume from day 10 to 14.

VEGFR2 levels in tumors of the nilotinib treatment group. The lowest values were recorded for tumors of the DC101 group, being significantly lower than in the nilotinib group ($P < .01$ for both time points). In the combined treatment group, the VEGFR2 levels were almost as high as in the controls, albeit at day 7, the difference to the nilotinib treatment group was significant (Figure 2*B*, $P < .05$, representative ultrasound images at day 7 and 14 are shown in Figure 2*A*).

Indirect immunofluorescence analysis of tumor sections at day 14 confirmed the highest VEGFR2-positive area fraction in nilotinib-treated tumors. The differences to the other treatment groups were significant, respectively (Figure 3*B*, $P < .001$ for all, examples of immunofluorescent staining are shown in Figure 3*A*). In further accordance with the ultrasound data, the lowest VEGFR2-positive area fraction was detected in the DC101 group, whereas in the combined treatment group, the VEGFR2-positive area fraction was almost similar as in the controls (Figure 3*B*). Analysis of the CD31-positive area fraction revealed also the highest microvessel density in tumors of the nilotinib treatment group, being significantly higher than in the other groups (Figure 3*C*, $P < .001$ for comparison with DC101 and combined group, $P < .01$ compared with controls). The lowest tumor vessel density was again found in the DC101 treatment group, the mean value being significantly lower than in the control group ($P < .05$). In the combined treatment group, the vessel density was slightly but not significantly lower than in the control group (Figure 3*C*). A rather similar trend could be observed when analyzing the amount of lectin-positive perfused, functional tumor vessels except for the combined group, though the differences between the groups were not significant and less prominent as compared to the VEGFR2 levels and the microvessel density (Supplementary Figure S1). The highest ratio of lectin-positive vessels per total vessel number was found in DC101-treated tumors.

Further analysis of the vascular structures by TPLSM of tumor sections at day 14 demonstrated an abnormal, irregular vascular network with various branching points in the control tumors (Figure 4). Nilotinib-treated tumors also exhibited an irregular vascular network, though the vessel density and the number of branching points were clearly higher than in the controls. In tumors of the DC101 group, vessel density and branching points were strongly reduced. Tumors of the combined treatment group had a slightly lower vessel density and number of branching points than the control tumors (Figure 4).

Reduced Vessel Maturity in Tumors After Nilotinib Treatment

The effects of the different treatments on vessel maturation were investigated by determining the ratio of α-SMA–positive vessels per total vessel number on tumor sections of day 14. The lowest percentage of α-SMA–positive vessels was detected in nilotinib-treated tumors, and the amount of mature vessel was markedly lower than in the controls, showing that vessel maturation was impaired by PDGFR inhibition (Figure 5*A*). In the DC101 and combined treatment group, the amount of mature tumor vessels was slightly lower than in the controls. The differences between the groups were not significant (Figure 5*A*).

We additionally analyzed myofibroblasts by determining the area fraction of non–vessel-associated α-SMA and the PDGFR-β–positive area fraction, respectively. The lowest amount of non–vessel-associated α-SMA–positive and of PDGFR-β–positive cells was detected in DC101-treated tumors (Figure 5, *B* and *C*). In tumors of the nilotinib treatment group, the mean values for non–vessel-associated α-SMA–positive and PDGFR-β–positive cells were only slightly lower than in the controls, whereas the mean values obtained for tumors of the combined treatment group ranged between the means of the nilotinib and DC101 group. Differences between the groups were not significant (Figure 5, *B* and *C*; representative immunofluorescent stainings are shown in *D*).

Nilotinib Inhibits Endothelial Tube Formation and Reduces Endothelial Cell Activity In Vitro

In order to investigate whether the increased tumor angiogenesis observed in response to nilotinib treatment *in vivo* was a direct or indirect effect of the drug, we analyzed the effects of nilotinib on angiogenesis *in vitro* using the endothelial tube formation assay. In contrast to the effects observed in the MCF-7 tumors *in vivo*, nilotinib exerted inhibitory effects on endothelial tube formation *in vitro* (Figure 6, *A* and *B*). At the higher dose, nilotinib completely blocked tube formation. In line with the blockade of *in vitro* angiogenesis, treatment of endothelial cells (HUVEC) with nilotinib in culture markedly reduced the mRNA expression of VEGFR2 and RAF1, confirming inhibitory effects of nilotinib on endothelial cell activity (Figure 6*C*).

Higher Expression of VEGF in Tumors After Treatment with Nilotinib

Due to the inhibitory effects of nilotinib on endothelial cell activation and tube formation *in vitro*, we assumed that the increased tumor angiogenesis observed *in vivo* was caused indirectly by effects of nilotinib on the tumor stroma or on the tumor cells. Since VEGF is a crucial mediator of angiogenesis, we analyzed the expression of VEGF in the stroma and in the tumor compartment. Immunofluorescent staining of tumor sections and quantification revealed slightly higher levels of murine VEGF in tumors treated with nilotinib as compared to the controls (Figure 7, *A* and *B*). The lowest values were obtained for the DC101 group. In the combined treatment group, murine VEGF levels were almost comparable to the controls. The differences between the groups were not significant (Figure 7*B*).

Analysis of human VEGF demonstrated a similar trend as observed for murine VEGF, but the differences between the treatment groups were stronger (Figure 7, *C* and *D*). The highest levels of tumor cell–derived VEGF were detected in nilotinib-treated tumors, being significantly increased as compared to the control ($P < .05$) and DC101 ($P < .01$) treatment group. The lowest VEGF expression was

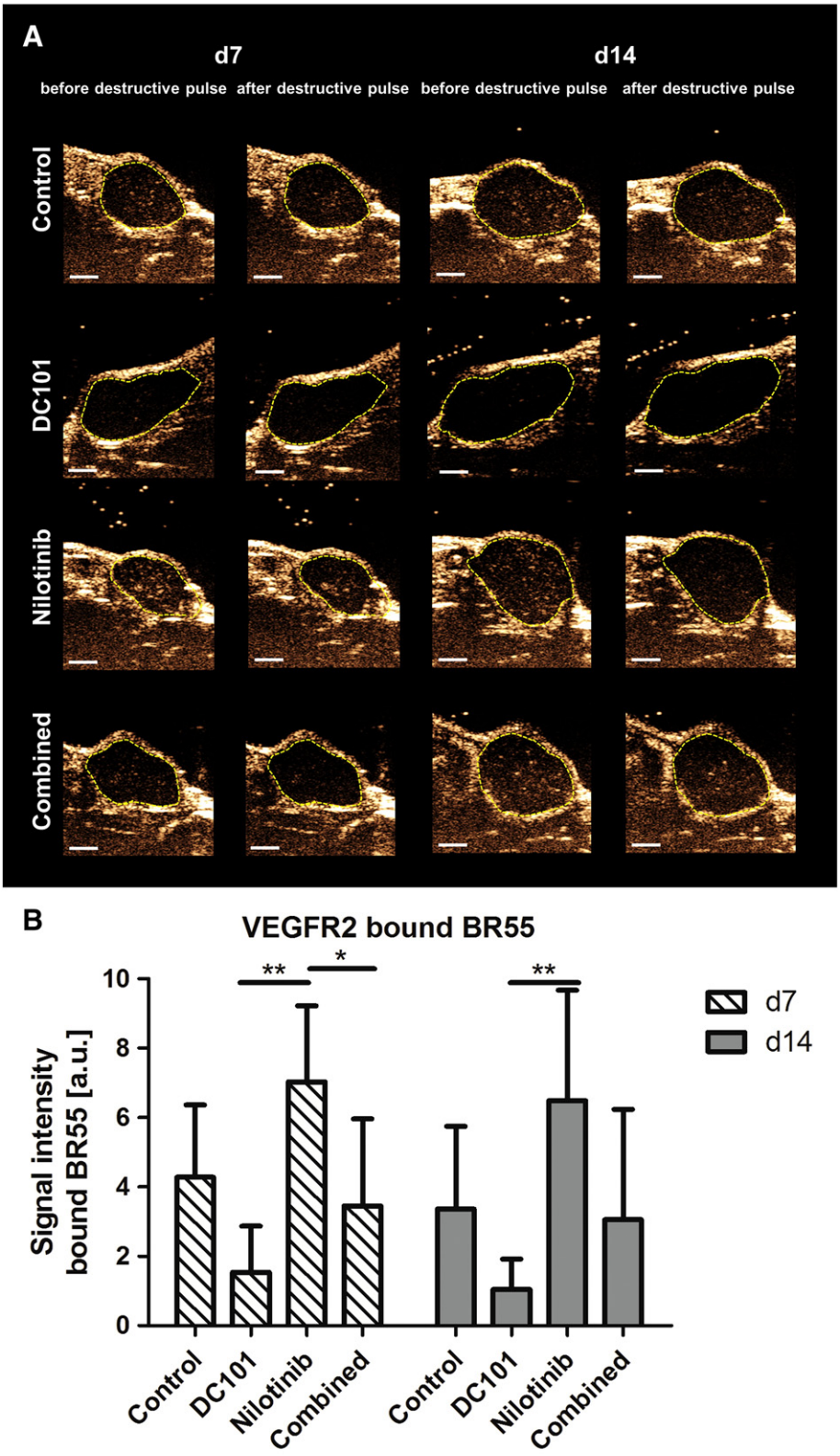

Figure 2. Nilotinib treatment enhances VEGFR2 expression. (A) Representative ultrasound images showing bound BR55 microbubbles in tumors of the control, DC101, nilotinib, and combined treatment groups at therapy day 7 and 14. Images were recorded shortly before (bound MBs + residual circulating MBs) and shortly after (residual circulating MBs) the destructive pulse in the central plane of the tumor. After implementation of a destructive pulse, markedly lower signal intensity can be seen in the tumor area (tumor encircled in yellow). Note the highest signal intensity of bound BR55 in the nilotinib-treated and the lowest signal intensity of bound microbubbles in the DC101-treated tumors. (B) Quantification of molecular ultrasound imaging signal revealed significantly higher VEGFR2 levels in the nilotinib than in the DC101 treatment group at day 7 and 14 (d7: $P = .0004$, d14: $P = .0024$). Additionally, the difference in VEGFR2 levels between the nilotinib and the combined treatment group was significant at day 7 ($P = .0252$). VEGFR2 expression was comparable in the combined and control treatment group. *$P < .05$; **$P < .01$; ***$P < .001$ (values presented as mean ± standard deviation).

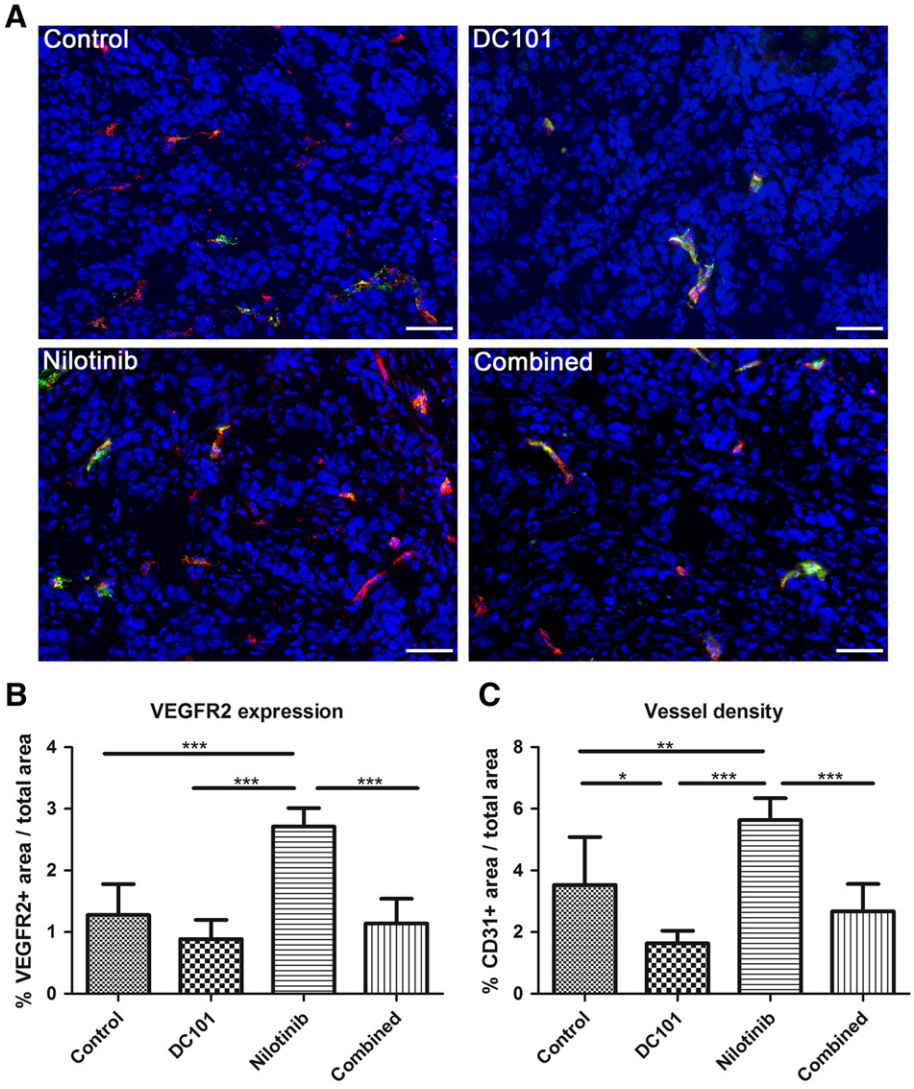

Figure 3. Nilotinib treatment enhances angiogenesis. (A) Representative immunostainings for VEGFR2- (red) and lectin-positive perfused vessels (green) in tumors of the control, DC101, nilotinib, and combined treatment group at day 14. Counterstaining of nuclei in blue; scale bar: 50 μm. (B) Quantification shows a significantly higher VEGFR2-positive area fraction in nilotinib-treated tumors in comparison to the control ($P = .0003$), DC101 ($P < .0001$), and combined ($P < .0001$) treatment group. The lowest mean value is detected in the DC101 group. The mean value of the combined group is almost comparable to the control group. (C) Quantification of the CD31-positive area fraction demonstrates a significantly higher microvessel density in tumors of nilotinib-treated mice as compared to tumors of the control ($P = .0127$), DC101 ($P < .0001$), and combined ($P < .0001$) treatment group. Additionally, a significant lower vessel density was observed in DC101-treated than in control tumors ($P = .0162$).

observed in tumors of the DC101 treatment group. In tumors of the combined treatment group, expression of VEGF by the tumor cells was slightly higher than in the control group. These findings indicated that, besides inhibiting vessel maturation, nilotinib had also direct effects on the tumor cells themselves.

Nilotinib Induces Upregulation of VEGF and IL-6 mRNA in MCF-7 Cells In Vitro

To analyze the direct effects of nilotinib on the tumor cells, we treated MCF-7 cells with nilotinib. Since growth of the breast carcinoma cells *in vivo* strictly depends on estrogen, the medium was supplemented with β-estradiol. Nilotinib was evaluated in different doses including lower doses as used for *in vitro* experiments on endothelial cells because, *in vivo*, lower doses are expected to reach the tumor cells as compared to the tumor vasculature. Nilotinib exerted stimulatory effects on the expression of VEGF mRNA (Figure 8*A*). Interestingly, strongest upregulation was observed for the lowest dose. In addition, a similar upregulation was found for the expression of IL-6 mRNA (Figure 8*B*). These findings strongly suggested that the enhanced expression of human VEGF protein in nilotinib-treated tumors was due to a direct effect of the drug on the tumor cells.

Discussion

In order to improve the efficacy of anti-VEGF/VEGFR treatment and the therapeutic outcome, PDGFR blockade has been suggested as supplemental therapeutic option with the aim to inhibit vessel maturation and to increase the number of vessels prone to VEGF/VEGFR-targeted therapy [5,6,31]. Thus, in the current study, we combined the VEGFR2 neutralizing antibody DC101 with nilotinib,

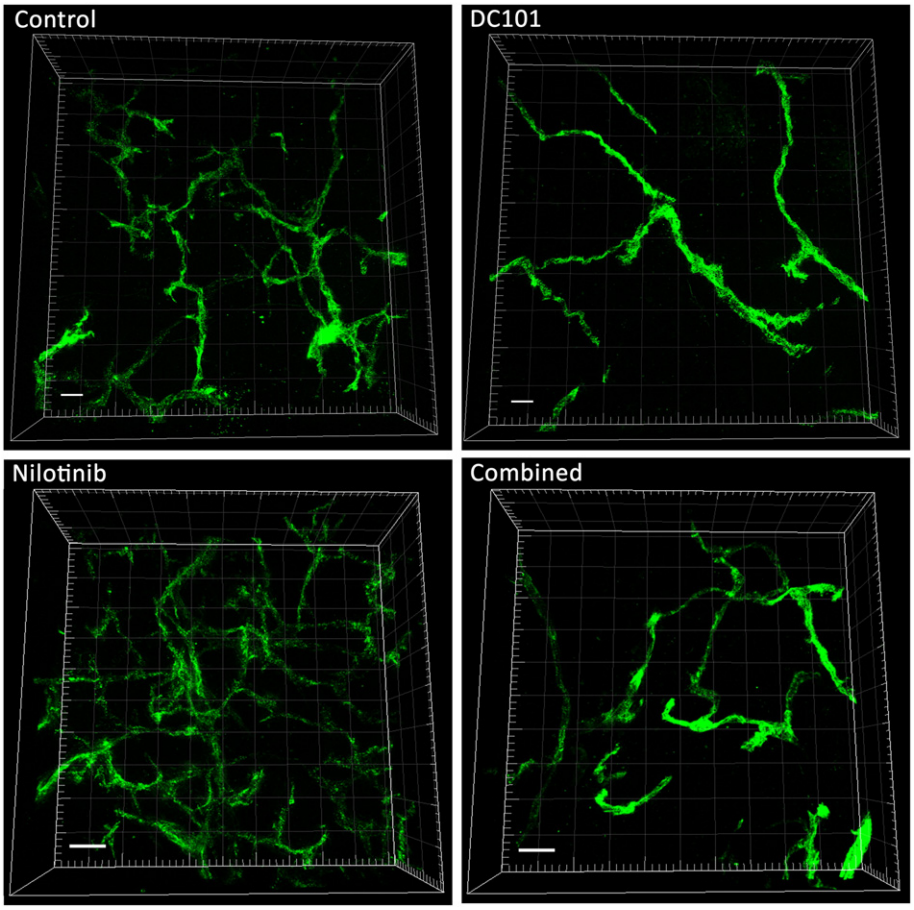

Figure 4. Nilotinib treatment leads to increased vessel sprouting. Representative TPLSM images of tumors from the different treatment groups at day 14 show the irregular vascular network with various branching points in the control, nilotinib, and combined treatment group. The nilotinib-treated tumor displays the highest vessel density and number of branch points. In the DC101-treated group, vessel density and the amount of branches are strongly reduced. Perfused vessels in green, scale bar: 50 μm.

a small tyrosine kinase inhibitor blocking the PDGFRs, for the treatment of orthotopic human breast carcinoma xenografts (MCF-7). For comparison, both agents were administered alone. MCF-7 tumors are characterized by a desmoplastic response involving α-SMA–positive myofibroblasts, comparable to human breast carcinomas. Furthermore, the amount of pericyte-associated, mature vessels is markedly increased when tumors exceed sizes of 4 mm in diameter [24]. Therefore, therapy was started at a tumor diameter of 3 to 4 mm.

In contrast to earlier studies describing an enhanced therapeutic efficacy by combining anti-VEGF/VEGFR therapy with blockade of vessel maturation [7,32], in our study, additional treatment with nilotinib did not enhance the effects of the VEGFR2 neutralizing antibody DC101. Tumor growth was almost similar in the combined and DC101 treatment group and only slightly lower than in the controls. Strongest inhibition of tumor angiogenesis was observed in response to sole treatment with DC101. This became obvious by the lowest VEGFR2 levels measured by molecular ultrasound imaging and was confirmed by immunohistological examinations. In contrast, nilotinib treatment did suppress vessel maturation but enhanced the VEGFR2 expression on the tumor endothelium and angiogenesis, resulting in the highest mean tumor volume at the end of the therapy. In the combined treatment group, the antiangiogenic effects of DC101 and the proangiogenic effects of nilotinib rather appeared counterbalanced since the VEGFR2 levels were similar as in the control tumors and the vessel density was only marginally lower. Additional *in vitro* analyses were performed in order to investigate the mechanism for the increased angiogenesis observed in tumors treated with nilotinib. Results were in contrast to the effects observed *in vivo* since nilotinib inhibited endothelial cell activation and tube formation. However, we assume that the inhibitory effect on the endothelial cells *in vitro* is rather due to inhibition of c-KIT and PDGFR-β than VEGFR2. This hypothesis is supported by the literature where angiogenesis blockade *via* c-KIT inhibition has been demonstrated for imatinib, which has comparable IC50 values towards tyrosine kinase activities of the c-KIT, PDGFR-β, and VEGFR2 receptors as nilotinib [33] Thus, the increased angiogenesis that was observed in the nilotinib-treated tumors *in vivo* was not induced by direct effects of the drug on the tumor endothelium but rather indirectly by effects of the drug on the stroma or the tumor cells. As VEGF plays a crucial role in tumor angiogenesis, we analyzed the VEGF protein levels in tumors of the different treatment groups. Whereas stromal VEGF expression was only slightly increased, tumor cell–derived VEGF was significantly enhanced in the nilotinib-treated tumors as compared to the other groups, indicating direct effects of nilotinib on the tumor cells. In line with the *in vivo* results, treatment of MCF-7 cells with nilotinib in cell culture showed upregulation of VEGF mRNA. In addition, we found a similar upregulation of IL-6

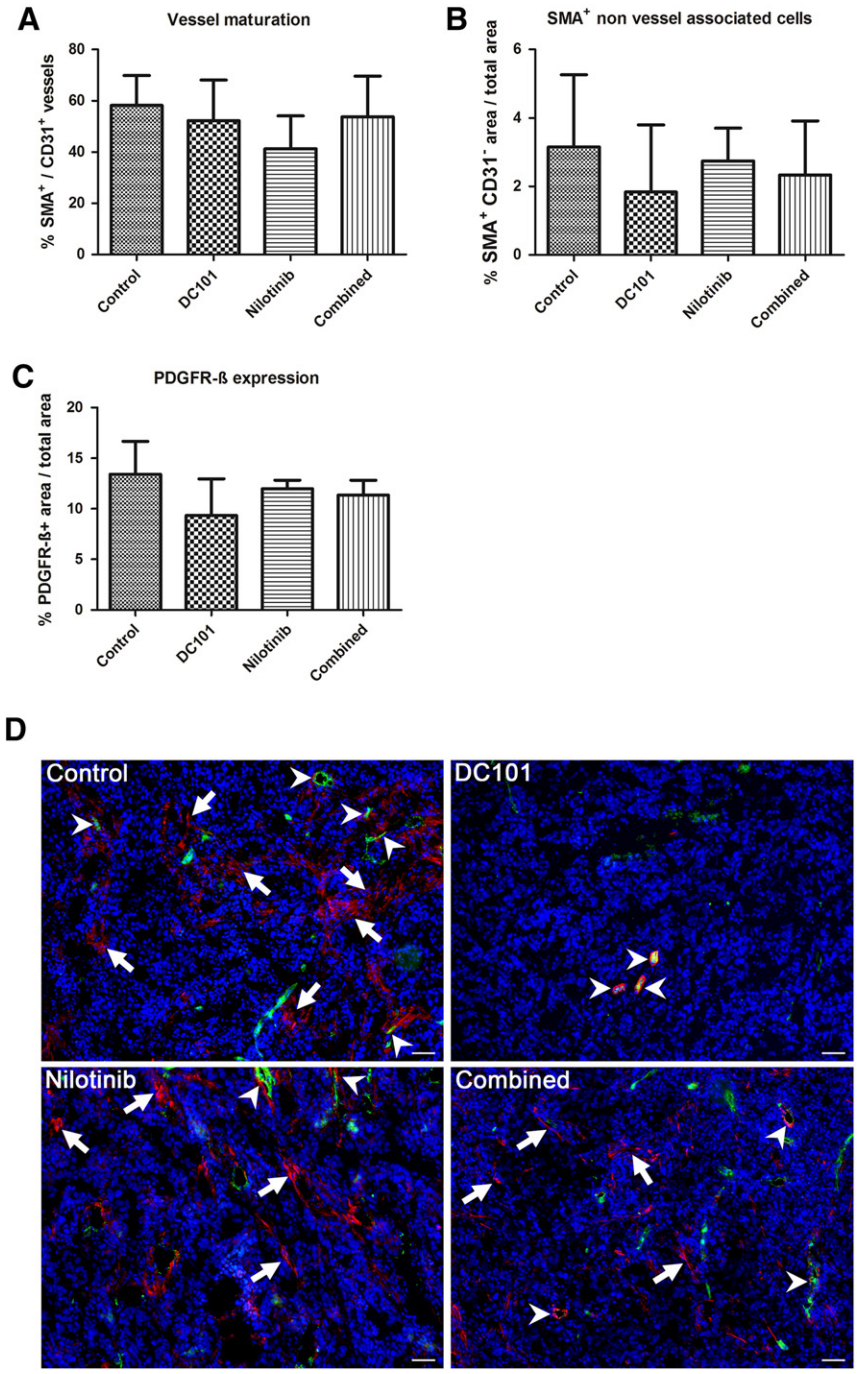

Figure 5. Lower vessel maturation in nilotinib-treated tumors and treatment effects on myofibroblasts. (A) Quantification reveals that the ratio of α-SMA–positive vessels per total vessel fraction is lowest in nilotinib-treated tumors showing an impaired vessel maturation by PDGFR inhibition. (B) The fraction of non–vessel-associated α-SMA–positive cells (myofibroblasts) is markedly reduced in DC101-treated tumors, whereas in tumors of the nilotinib group, the amount of non–vessel-associated α-SMA–positive cells is only slightly lower than in the controls. (C) Quantification of the PDGFR-β–positive area fraction reveals a similar trend as for non–vessel-associated α-SMA, showing the lowest value for the DC101 treatment group, whereas the mean value for nilotinib-treated tumors is almost as high as in the controls. Data are presented as mean values ± standard deviation. (D) Representative immunofluorescent staining for α-SMA (red) and CD31 (green) in tumors of the control, DC101, nilotinib, and combined treatment groups at day 14. Counterstaining of nuclei in blue; arrows show non–vessel-associated α-SMA–positive cells, and arrowheads represent α-SMA–positive mature vessels. Scale bar: 50 μm.

mRNA, a cytokine which was also shown to exert proangiogenic effects [34]. These findings can provide an explanation for the increased angiogenesis that was observed in the nilotinib-treated tumors *in vivo*.

The enhanced expression of VEGF and IL-6 in MCF-7 cells treated with nilotinib is in contrast to findings in literature where inhibitory effects of nilotinib and imatinib on tumor cells are described [35–38]. However, these studies were predominantly performed with higher doses of nilotinib than the concentrations that we used for MCF-7 treatment. Interestingly, in our *in vitro* experiments, the highest mRNA levels of VEGF and IL-6 were

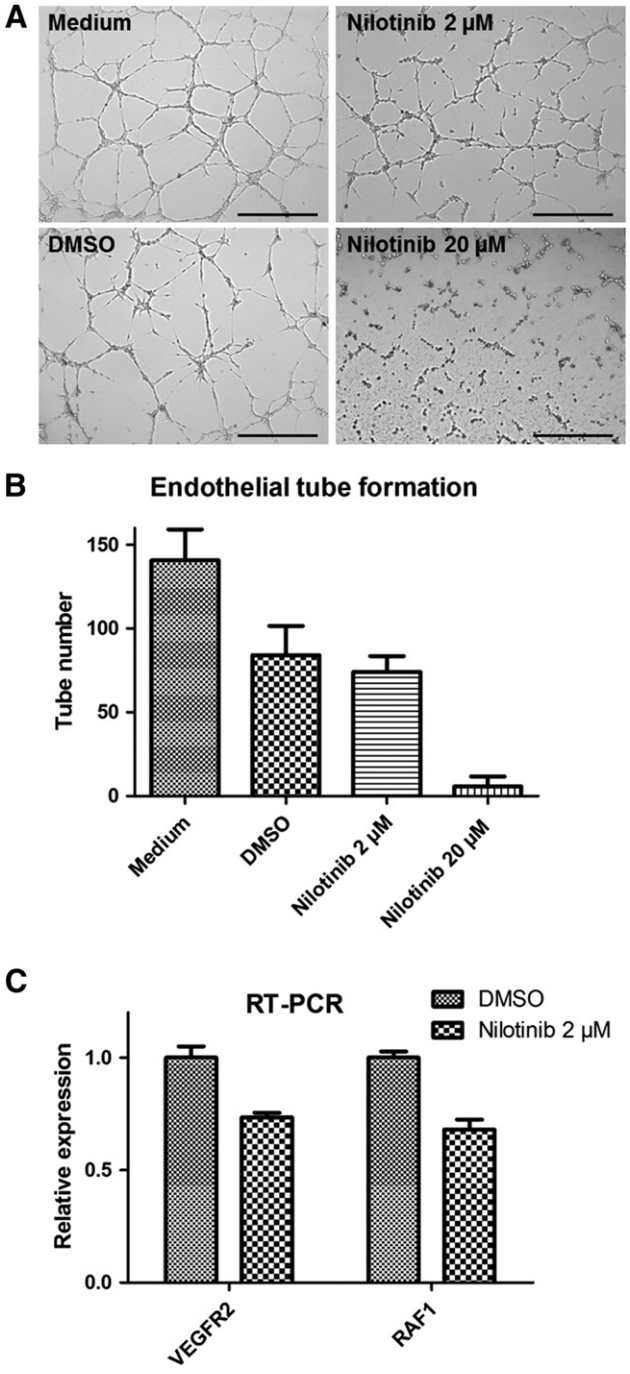

Figure 6. Nilotinib treatment inhibits angiogenesis *in vitro*. (A) Representative pictures of the endothelial tube formation assay after incubation with medium, medium containing DMSO (2%), and different concentrations of nilotinib (2 and 20 μM). Note the complete inhibition of endothelial tube formation with the higher dose of nilotinib. (B) Quantification shows a slightly lower number of endothelial tubes after treatment with 2 μM of nilotinib as compared to the DMSO control and a strongly reduced number of tubes after treatment with 20 μM of nilotinib. Data are presented as mean values ± standard deviation. Scale bar: 500 μm. (C) qRT-PCR analysis of HUVEC treated with nilotinib (2 μM) shows downregulation of VEGFR2 and RAF1 mRNA.

measured in MCF-7 cells after treatment with the lowest dose. Thus, there seems to be a concentration window in which nilotinib does not strongly inhibit tumor cell survival but significantly induces VEGF and IL-6 mRNA expression. *In vivo*, such concentrations may be present in MCF-7 tumors that are highly desmoplastic and are characterized by a low vascularization.

While, in our study, additional nilotinib treatment had no beneficial effects on the antiangiogenic therapy with the VEGFR2-blocking antibody despite inhibition of vessel maturation, Bergers and colleagues observed a strong reduction in tumor vascularization and an improved therapeutic outcome when combining VEGFR and PDGFR inhibitors in a pancreatic islet carcinogenesis model [7]. Other groups also found an enhanced vessel regression, in part associated with diminished tumor growth, when combining VEGF/VEGFR-targeting therapy with agents that block vessel maturation [8,39–41]. On the other hand, adverse effects of drugs that target PDGFR signaling have been described in literature. In another breast carcinoma xenograft model, Rappa and colleagues observed an increased tumor take rate and a faster tumor growth after treating the mice with imatinib [42]. In a clinical trial in patients with advanced renal cell carcinoma, combined VEGFR and PDGFR inhibition did not improve the therapeutic outcome but instead increased the side effects such as diarrhea, eczema, or fatigue [43]. Moreover, impairment of vessel maturation can promote tumor metastasis. Deficient pericyte recruitment or perturbations of pericyte-endothelial cell interactions were shown to increase metastatic dissemination of tumor cells in a transgenic model of pancreatic islet cancer [44]. In accordance with these preclinical data, a correlation was found between the absence of pericytes in tumor vessels and metastasis in human colorectal cancer patients [45]. Further preclinical studies are needed to clarify the potential benefits and risks associated with therapies targeting PDGFR signaling and vessel maturation. In addition, the treatment schedule might influence the outcome of PDGFR- and VEGFR-targeting therapies. In this regard, initially performing PDGFR signaling blockade for a defined period of time might be favorable in order to interfere with blood vessel maturation and to make the vessels more prone to antiangiogenic therapy. Subsequent monotherapy with a VEGF/VEGFR-targeting drug might then more efficiently prune tumor vessels due to their immature status. Such an intermittent treatment scheme might also lead to normalization of the VEGF levels after cessation of nilotinib treatment which would be favorable for the subsequent VEGFR2 blockade. Nevertheless, the doses and the time window for each therapeutic regimen have to be well evaluated in order to improve the outcome.

Interestingly, the strongest reduction in myofibroblasts was observed in DC101-treated tumors, whereas in nilotinib-treated tumors, the amount of myofibroblasts was only marginally lower than in the controls despite PDGFR inhibition. One possible explanation might be that since we started with the therapy when tumors had reached a size of 3 to 4 mm in diameter, myofibroblasts and pericytes might have already been recruited to the tumor. Thus, nilotinib did not affect their recruitment but inhibited the association of pericytes with the endothelial cells. A similar reduction in α-SMA– and PDGFR-β–positive myofibroblasts after DC101 treatment was observed in other tumor models [46,47], pointing towards stromal normalization and a decrease in stromal density in response to the antiangiogenic treatment.

These controversial results indicate that responses of such combination therapies in the clinics can be expected to be heterogeneous. Therefore, careful and mechanism-related monitoring may be required, which raises the demand for new and more specific

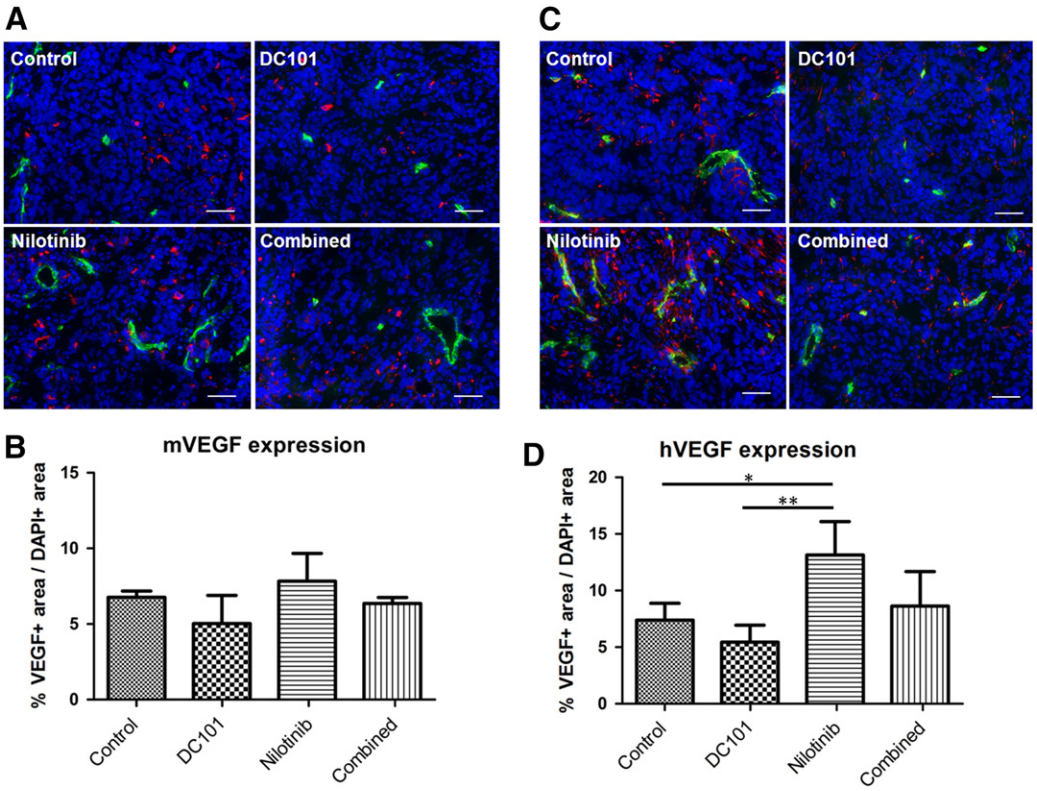

Figure 7. Increased VEGF levels in tumors after treatment with nilotinib *in vivo*. (A) Representative immunostainings for murine VEGF (red) of the control, DC101, nilotinib, and combined treatment group at day 14. Counterstaining of nuclei in blue; lectin-positive vessels in green. Scale bar: 50 μm. (B) Quantification of VEGF stainings (ratio VEGF+ area/DAPI+ area) shows slightly increased levels of murine VEGF in tumors of the nilotinib as compared to the control and combined treatment group. The lowest levels are recorded for DC101-treated tumors. (C) Representative immunostainings for human VEGF (red) of tumor sections at day 14 show markedly enhanced expression in nilotinib-treated tumors. Counterstaining of nuclei in blue; lectin-positive vessels in green. Scale bar: 50 μm. (D) Quantification confirms significantly enhanced levels of human VEGF in tumors of the nilotinib as compared to the control ($P = .0133$) and DC101 treatment group ($P = .0036$).

imaging tools. In our study, the effects of the different treatments on tumor angiogenesis were noninvasively analyzed by molecular ultrasound imaging using the clinically used VEGFR2-targeted microbubbles (BR55). The molecular ultrasound data showed a very good agreement with the immunohistological data on VEGFR2 expression after tumor resection. These findings provide further evidence that molecular ultrasound imaging using BR55 microbubbles and the destruction-replenishing method is highly suitable for investigating tumor angiogenesis and therapy effects noninvasively *in vivo*. In previous investigations including studies performed by our group, molecular ultrasound imaging with BR55 has shown a high sensitivity and accuracy for the noninvasive characterization of breast and liver tumors and with respect to the early assessment of therapy effects [22,23,25,26,29,46,48].

In summary, the results of this study indicate that nilotinib treatment can be unfavorable in desmoplastic breast tumors as it can promote tumor angiogenesis and counteract the effects of antiangiogenic therapy targeting VEGF/VEGFR signaling.

Supplementary data to this article can be found online at http://dx.doi.org/10.1016/j.neo.2017.08.009.

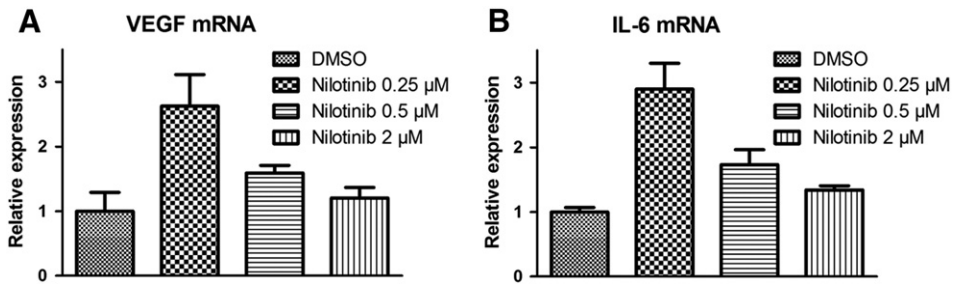

Fig. 8. Nilotinib treatment leads to upregulation of VEGF and IL-6 mRNA in MCF-7 cells *in vitro*. qRT-PCR analysis shows that the expression of VEGF mRNA (A) and IL-6 mRNA (B) is increased in MCF-7 cells after treatment with nilotinib in different doses. For both VEGF and IL-6 mRNA, strongest upregulation is observed with the lowest dose of nilotinib (0.25 μM).

Disclosure of Potential Conflicts of Interest

Fabian Kiessling was consulted for Bracco. Isabelle Tardy and Sybille Pochon were employees of Bracco.

Acknowledgements

This study was supported by Bracco.

References

[1] Shibuya M (2006). Differential roles of vascular endothelial growth factor receptor-1 and receptor-2 in angiogenesis. *J Biochem Mol Biol* **39**, 469–478.

[2] Casanovas O, Hicklin DJ, Bergers G, and Hanahan D (2005). Drug resistance by evasion of antiangiogenic targeting of VEGF signaling in late-stage pancreatic islet tumors. *Cancer Cell* **8**, 299–309.

[3] Bergers G and Hanahan D (2008). Modes of resistance to anti-angiogenic therapy. *Nat Rev Cancer* **8**, 592–603.

[4] Paez-Ribes M, Allen E, Hudock J, Takeda T, Okuyama H, Vinals F, Inoue M, Bergers G, Hanahan D, and Casanovas O (2009). Antiangiogenic therapy elicits malignant progression of tumors to increased local invasion and distant metastasis. *Cancer Cell* **15**, 220–231.

[5] Benjamin LE, Hemo I, and Keshet E (1998). A plasticity window for blood vessel remodelling is defined by pericyte coverage of the preformed endothelial network and is regulated by PDGF-B and VEGF. *Development* **125**, 1591–1598.

[6] Benjamin LE, Golijanin D, Itin A, Pode D, and Keshet E (1999). Selective ablation of immature blood vessels in established human tumors follows vascular endothelial growth factor withdrawal. *J Clin Invest* **103**, 159–165.

[7] Bergers G, Song S, Meyer-Morse N, Bergsland E, and Hanahan D (2003). Benefits of targeting both pericytes and endothelial cells in the tumor vasculature with kinase inhibitors. *J Clin Invest* **111**, 1287–1295.

[8] Erber R, Thurnher A, Katsen AD, Groth G, Kerger H, Hammes HP, Menger MD, Ullrich A, and Vajkoczy P (2004). Combined inhibition of VEGF and PDGF signaling enforces tumor vessel regression by interfering with pericyte-mediated endothelial cell survival mechanisms. *FASEB J* **18**, 338–340.

[9] Barrett T, Brechbiel M, Bernardo M, and Choyke PL (2007). MRI of tumor angiogenesis. *J Magn Reson Imaging* **26**, 235–249.

[10] Cai W and Chen X (2008). Multimodality molecular imaging of tumor angiogenesis. *J Nucl Med* **49**(Suppl. 2), 113S–128S.

[11] Lederle W, Palmowski M, and Kiessling F (2012). Imaging in the age of molecular medicine: monitoring of anti-angiogenic treatments. *Curr Pharm Biotechnol* **13**, 595–608.

[12] Iagaru A and Gambhir SS (2013). Imaging tumor angiogenesis: the road to clinical utility. *AJR Am J Roentgenol* **201**, W183–191.

[13] Kiessling F, Fokong S, Bzyl J, Lederle W, Palmowski M, and Lammers T (2014). Recent advances in molecular, multimodal and theranostic ultrasound imaging. *Adv Drug Deliv Rev* **72**, 15–27.

[14] Abou-Elkacem L, Bachawal SV, and Willmann JK (2015). Ultrasound molecular imaging: Moving toward clinical translation. *Eur J Radiol* **84**, 1685–1693.

[15] Kiessling F, Huppert J, and Palmowski M (2009). Functional and molecular ultrasound imaging: concepts and contrast agents. *Curr Med Chem* **16**, 627–642.

[16] Guibal A, Taillade L, Mule S, Comperat E, Badachi Y, Golmard JL, Le Guillou-Buffello D, Rixe O, Bridal SL, and Lucidarme O (2010). Noninvasive contrast-enhanced US quantitative assessment of tumor microcirculation in a murine model: effect of discontinuing anti-VEGF therapy. *Radiology* **254**, 420–429.

[17] Korpanty G, Carbon JG, Grayburn PA, Fleming JB, and Brekken RA (2007). Monitoring response to anticancer therapy by targeting microbubbles to tumor vasculature. *Clin Cancer Res* **13**, 323–330.

[18] Palmowski M, Huppert J, Ladewig G, Hauff P, Reinhardt M, Mueller MM, Woenne EC, Jenne JW, Maurer M, and Kauffmann GW, et al (2008). Molecular profiling of angiogenesis with targeted ultrasound imaging: early assessment of antiangiogenic therapy effects. *Mol Cancer Ther* **7**, 101–109.

[19] Deshpande N, Ren Y, Foygel K, Rosenberg J, and Willmann JK (2011). Tumor angiogenic marker expression levels during tumor growth: longitudinal assessment with molecularly targeted microbubbles and US imaging. *Radiology* **258**, 804–811.

[20] Kiessling F, Fokong S, Koczera P, Lederle W, and Lammers T (2012). Ultrasound microbubbles for molecular diagnosis, therapy, and theranostics. *J Nucl Med* **53**, 345–348.

[21] Willmann JK, Paulmurugan R, Chen K, Gheysens O, Rodriguez-Porcel M, Lutz AM, Chen IY, Chen X, and Gambhir SS (2008). US imaging of tumor angiogenesis with microbubbles targeted to vascular endothelial growth factor receptor type 2 in mice. *Radiology* **246**, 508–518.

[22] Pysz MA, Foygel K, Rosenberg J, Gambhir SS, Schneider M, and Willmann JK (2010). Antiangiogenic cancer therapy: monitoring with molecular US and a clinically translatable contrast agent (BR55). *Radiology* **256**, 519–527.

[23] Pochon S, Tardy I, Bussat P, Bettinger T, Brochot J, von Wronski M, Passantino L, and Schneider M (2010). BR55: a lipopeptide-based VEGFR2-targeted ultrasound contrast agent for molecular imaging of angiogenesis. *Invest Radiol* **45**, 89–95.

[24] Bzyl J, Palmowski M, Rix A, Arns S, Hyvelin JM, Pochon S, Ehling J, Schrading S, Kiessling F, and Lederle W (2013). The high angiogenic activity in very early breast cancer enables reliable imaging with VEGFR2-targeted microbubbles (BR55). *Eur Radiol* **23**, 468–475.

[25] Bachawal SV, Jensen KC, Lutz AM, Gambhir SS, Tranquart F, Tian L, and Willmann JK (2013). Earlier detection of breast cancer with ultrasound molecular imaging in a transgenic mouse model. *Cancer Res* **73**, 1689–1698.

[26] Baetke SC, Rix A, Tranquart F, Schneider R, Lammers T, Kiessling F, and Lederle W (2016). Squamous cell carcinoma xenografts: use of VEGFR2-targeted microbubbles for combined functional and molecular US to monitor antiangiogenic therapy effects. *Radiology* **278**, 430–440.

[27] Weisberg E, Manley PW, Breitenstein W, Bruggen J, Cowan-Jacob SW, Ray A, Huntly B, Fabbro D, Fendrich G, and Hall-Meyers E, et al (2005). Characterization of AMN107, a selective inhibitor of native and mutant Bcr-Abl. *Cancer Cell* **7**, 129–141.

[28] Kim IK, Rhee CK, Yeo CD, Kang HH, Lee DG, Lee SH, and Kim JW (2013). Effect of tyrosine kinase inhibitors, imatinib and nilotinib, in murine lipopolysaccharide-induced acute lung injury during neutropenia recovery. *Crit Care* **17**, R114.

[29] Bzyl J, Lederle W, Rix A, Grouls C, Tardy I, Pochon S, Siepmann M, Penzkofer T, Schneider M, and Kiessling F, et al (2011). Molecular and functional ultrasound imaging in differently aggressive breast cancer xenografts using two novel ultrasound contrast agents (BR55 and BR38). *Eur Radiol* **21**, 1988–1995.

[30] Lederle W, Linde N, Heusel J, Bzyl J, Woenne EC, Zwick S, Skobe M, Kiessling F, Fusenig NE, and Mueller MM (2010). Platelet-derived growth factor-B normalizes micromorphology and vessel function in vascular endothelial growth factor-A–induced squamous cell carcinomas. *Am J Pathol* **176**, 981–994.

[31] Hellstrom M, Kalen M, Lindahl P, Abramsson A, and Betsholtz C (1999). Role of PDGF-B and PDGFR-beta in recruitment of vascular smooth muscle cells and pericytes during embryonic blood vessel formation in the mouse. *Development* **126**, 3047–3055.

[32] Huang Y, Stylianopoulos T, Duda DG, Fukumura D, and Jain RK (2013). Benefits of vascular normalization are dose and time dependent—letter. *Cancer Res* **73**, 7144–7146.

[33] Matsui J, Wakabayashi T, Asada M, Yoshimatsu K, and Okada M (2004). Stem cell factor/c-kit signaling promotes the survival, migration, and capillary tube formation of human umbilical vein endothelial cells. *J Biol Chem* **279**, 18600–18607.

[34] Huang S-P, Wu M-S, Shun C-T, Wang H-P, Lin M-T, Kuo M-L, and Lin J-T (2004). Interleukin-6 increases vascular endothelial growth factor and angiogenesis in gastric carcinoma. *J Biomed Sci* **11**, 517–527.

[35] Litz J and Krystal GW (2006). Imatinib inhibits c-Kit–induced hypoxia-inducible factor-1α activity and vascular endothelial growth factor expression in small cell lung cancer cells. *Mol Cancer Ther* **5**, 1415–1422.

[36] Schultz JD, Rotunno S, Riedel F, Anders C, Erben P, Hofheinz RD, Faber A, Thorn C, Sommer JU, and Hörmann K, et al (2011). Synergistic effects of imatinib and carboplatin on VEGF, PDGF and PDGF-Rα/β expression in squamous cell carcinoma of the head and neck in vitro. *Int J Oncol* **38**, 1001–1012.

[37] Kadivar A, Kamalidehghan B, Akbari Javar H, Karimi B, Sedghi R, and Noordin MI (2017). Antiproliferation effect of imatinib mesylate on MCF7, T-47D tumorigenic and MCF 10A nontumorigenic breast cell lines via PDGFR-β. *Drug Des Devel Ther* **11**, 469–481.

[38] Archibald M, Pritchard T, Nehoff H, Rosengren RJ, Greish K, and Taurin S (2016). A combination of sorafenib and nilotinib reduces the growth of castrate-resistant prostate cancer. *Int J Nanomedicine* **11**, 179–200.

[39] Shaheen RM, Tseng WW, Davis DW, Liu W, Reinmuth N, Vellagas R, Wieczorek AA, Ogura Y, McConkey DJ, and Drazan KE, et al (2001). Tyrosine kinase inhibition of multiple angiogenic growth factor receptors improves survival in mice bearing colon cancer liver metastases by inhibition of endothelial cell survival mechanisms. *Cancer Res* **61**, 1464–1468.

[40] Reinmuth N, Liu W, Jung YD, Ahmad SA, Shaheen RM, Fan F, Bucana CD, McMahon G, Gallick GE, and Ellis LM (2001). Induction of VEGF in

perivascular cells defines a potential paracrine mechanism for endothelial cell survival. *FASEB J* **15**, 1239–1241.

[41] Farhadi MR, Capelle HH, Erber R, Ullrich A, and Vajkoczy P (2005). Combined inhibition of vascular endothelial growth factor and platelet-derived growth factor signaling: effects on the angiogenesis, microcirculation, and growth of orthotopic malignant gliomas. *J Neurosurg* **102**, 363–370.

[42] Rappa G, Anzanello F, and Lorico A (2011). Imatinib mesylate enhances the malignant behavior of human breast carcinoma cells. *Cancer Chemother Pharmacol* **67**, 919–926.

[43] Hainsworth JD, Spigel DR, Sosman JA, Burris III HA, Farley C, Cucullu H, Yost K, Hart LL, Sylvester L, and Waterhouse DM, et al (2007). Treatment of advanced renal cell carcinoma with the combination bevacizumab/erlotinib/imatinib: a phase I/II trial. *Clin Genitourin Cancer* **5**, 427–432.

[44] Xian X, Hakansson J, Stahlberg A, Lindblom P, Betsholtz C, Gerhardt H, and Semb H (2006). Pericytes limit tumor cell metastasis. *J Clin Invest* **116**, 642–651.

[45] Yonenaga Y, Mori A, Onodera H, Yasuda S, Oe H, Fujimoto A, Tachibana T, and Imamura M (2005). Absence of smooth muscle actin-positive pericyte coverage of tumor vessels correlates with hematogenous metastasis and prognosis of colorectal cancer patients. *Oncology* **69**, 159–166.

[46] Vosseler S, Mirancea N, Bohlen P, Mueller MM, and Fusenig NE (2005). Angiogenesis inhibition by vascular endothelial growth factor receptor-2 blockade reduces stromal matrix metalloproteinase expression, normalizes stromal tissue, and reverts epithelial tumor phenotype in surface heterotransplants. *Cancer Res* **65**, 1294–1305.

[47] Smith NR, Baker D, Farren M, Pommier A, Swann R, Wang X, Mistry S, McDaid K, Kendrew J, and Womack C, et al (2013). Tumor stromal architecture can define the intrinsic tumor response to VEGF-targeted therapy. *Clin Cancer Res* **19**, 6943–6956.

[48] Bzyl J, Lederle W, Palmowski M, and Kiessling F (2012). Molecular and functional ultrasound imaging of breast tumors. *Eur J Radiol* **81**(Suppl. 1), S11–12.